FIGURE 1

Recirculating Adsorption Test Apparatus

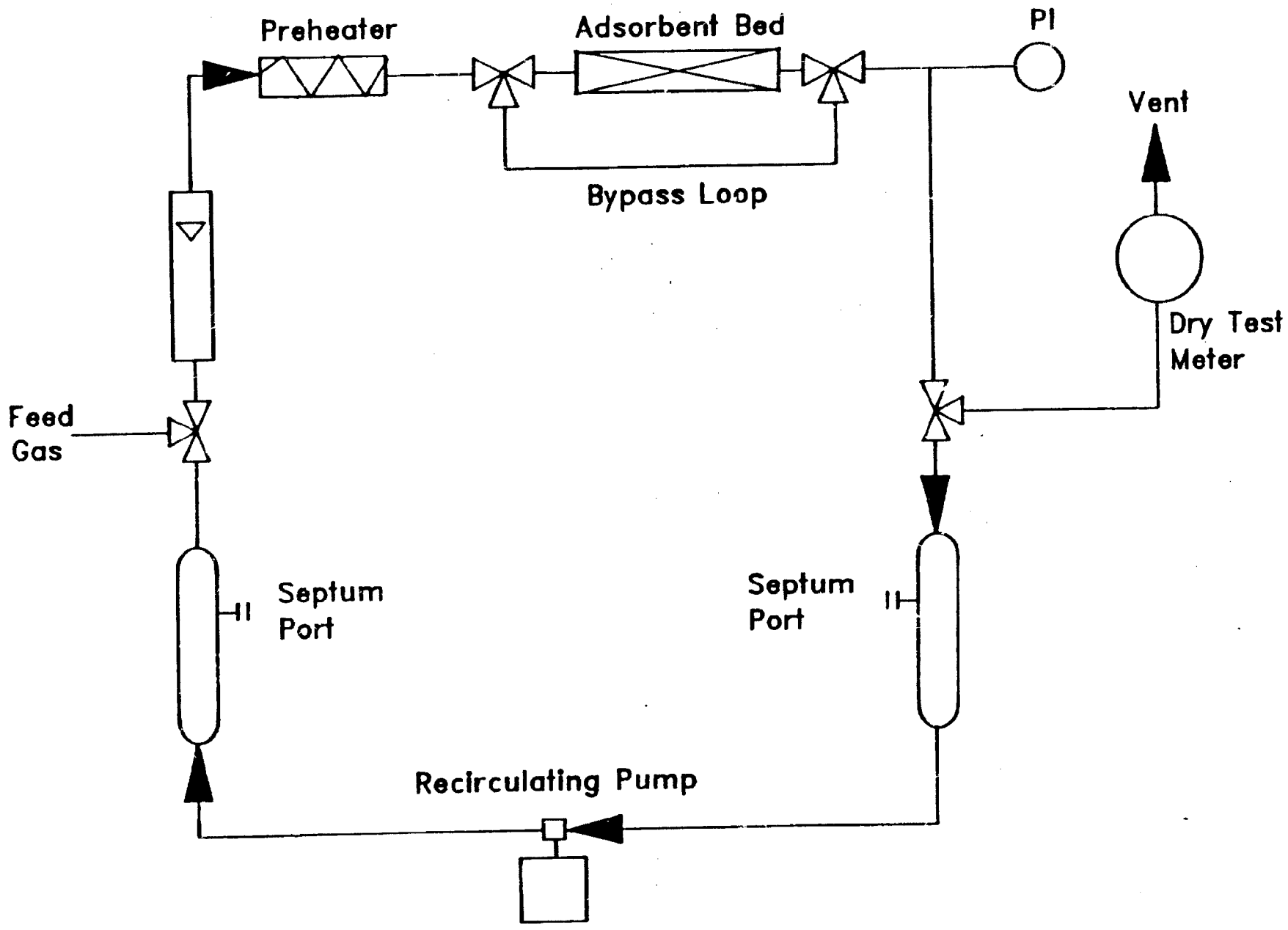

All gases vented from the system are scrubbed through a bubbler system or a heated packed bed to decompose the poisons in the gas stream. In the case of iron and nickel carbonyls, this consists of passing the gas stream through a 6 to 10 inch bed of alumina heated to 300°C. This decomposes the metal carbonyls liberating carbon monoxide and depositing iron or nickel metal on the alumina. Carbonyl sulfide and hydrogen sulfide are scrubbed through a bubbler system filled with two molar sodium hydroxide and phenolpthalein indicator. This converts the material to sodium sulfide and water. Similarly, hydrogen chloride is scrubbed through a two molar solution of sodium hydroxide, producing sodium chloride and water on decomposition.

The recirculating adsorption apparatus is equipped with three heated zones: a preheater, adsorption bed heater, and a bar heater. Each is controlled by an ECS controller and alarm card. There is a high/low pressure alarm in the recirculating loop configured to shut down the pump, solenoid, and heated zones should pressures drop below 25 psi or exceed 105 psi. A hood failure alarm of the differential pressure sensing type continuously monitors air flow through the hood. In the event of a failure, an audible alarm sounds and the power to the solenoid on the pump nitrogen supply line and ASCO solenoid on the poison feed line is interrupted.

A typical experiment in the recirculating apparatus was run as follows:

1. A sample of adsorbent was regenerated with nitrogen at 150 to 400°C (dependent upon the adsorbent) to a dew point of less than -40°C while in the adsorption bed.

2. Using the inlet feed system, the adsorption loop was pressurized to 90 psig with carbon dioxide and isolated.

3. The recirculating loop was then vented to atmospheric pressure. The loop was closed, filled with 1 atmosphere of trace impurity, and finally filled to 90 psig with carbon dioxide. In the actual pretreatment bed, the impurities wi be adsorbed from a synthesis gas matrix (CO, H_2, N_2, CO_2). For experimental simplification, all runs were done with CO_2 only Since CO_2 is the most strongly adsorbed of all the components in the matrix, the data obtained from CO_2 should provide a good estimate of capacities in the actual synthesis gas matrix. The pressure of 90 psig was chosen because it reflects tne partial pressure of CO_2 at process operating conditions.

4. After recirculating for about 10 minutes to ensure good mixing, the concentration in the recirculating loop was determined by withdrawing a 1 cc sample at the sampling port and injecting into the gas chromatograph. The GC employed in this study was a Hewlett Packard 5890A. The volume of the sample withdrawn (1 cc) was much less than the total system volume (4 liters). In the case of HCl, continuous on-line analysis was done using a Nicolet 1000 meter cell FTIR installed directly in the recirculating loop. The system volume was 9 liters.

5. Once the concentration in the recirculating loop was known, the gas was directed to the adsorption bed with valves V-16 and V-17.

6. The impurity concentration in the gas stream was then monitored as a function of time yielding data on the kinetics of adsorption.

7. After equilibrium was reached and the final impurity concentration was known, the adsorption bed was isolated using valves V-16 and V-17.

8. Another adsorption point or desorption point was obtained by increasing or decreasing the impurity concentration in the recirculating loop and following step 3-7. The adsorbate concentration in the recirculating loop was decreased by purging with CO_2.

Analytical Techniques

A packed column gas chromatograph equipped with an electron capture detector (ECD) was used to analyze both nickel and iron carbonyl. For determination of COS and H_2S, a packed column gas chromatograph equipped with a photoionization detector (PID) was employed. Specifics about the analytical techniques including column packings, carrier gas flowrates, temperatures as well as sample chromatograms for carbonyl and sulfur determination are given in Appendix A.

RESULTS AND DISCUSSION:

Adsorption of $Fe(CO)_5$

Equilibrium Capacity of Various Adsorbents at 100°F

A number of commercially available adsorbents were screened for their $Fe(CO)_5$ adsorption capacity at 100°F and 40 psig (5% CO, 95% N_2). These adsorbents included three activated carbons, silica gel, activated alumina, H-Y zeolite, and spent methanol catalyst. Some of the pertinent physical properties of these adsorbents are given in Table 2.

The $Fe(CO)_5$ adsorption isotherms on the seven adsorbents screened initially are given in Figure 2. As clearly noted from the isotherms, the activated carbons and the zeolite show significantly higher adsorption capacities than silica gel, alumina, or spent methanol catalyst. Consequently, the activated carbons and H-Y zeolites were further screened for $Fe(CO)_5$ removal. Several variables including the effect of temperature, total carrier gas pressure, and thermal regenerability of the adsorbents were investigated.

It is interesting to note that the $Fe(CO)_5$ capacity and Henry's law constants (initial isotherm slopes) for the adsorbents increase as the surface area of the adsorbent increases. As the microporosity of an adsorbent increases so does its surface area, thus the adsorption capacity for $Fe(CO)_5$ is also enhanced. This is true for adsorbents with very different surface polarities like carbons and zeolites. This suggests that adsorption of

FIGURE 2

Fe(CO)5 adsorption at 100 F. 40 psig

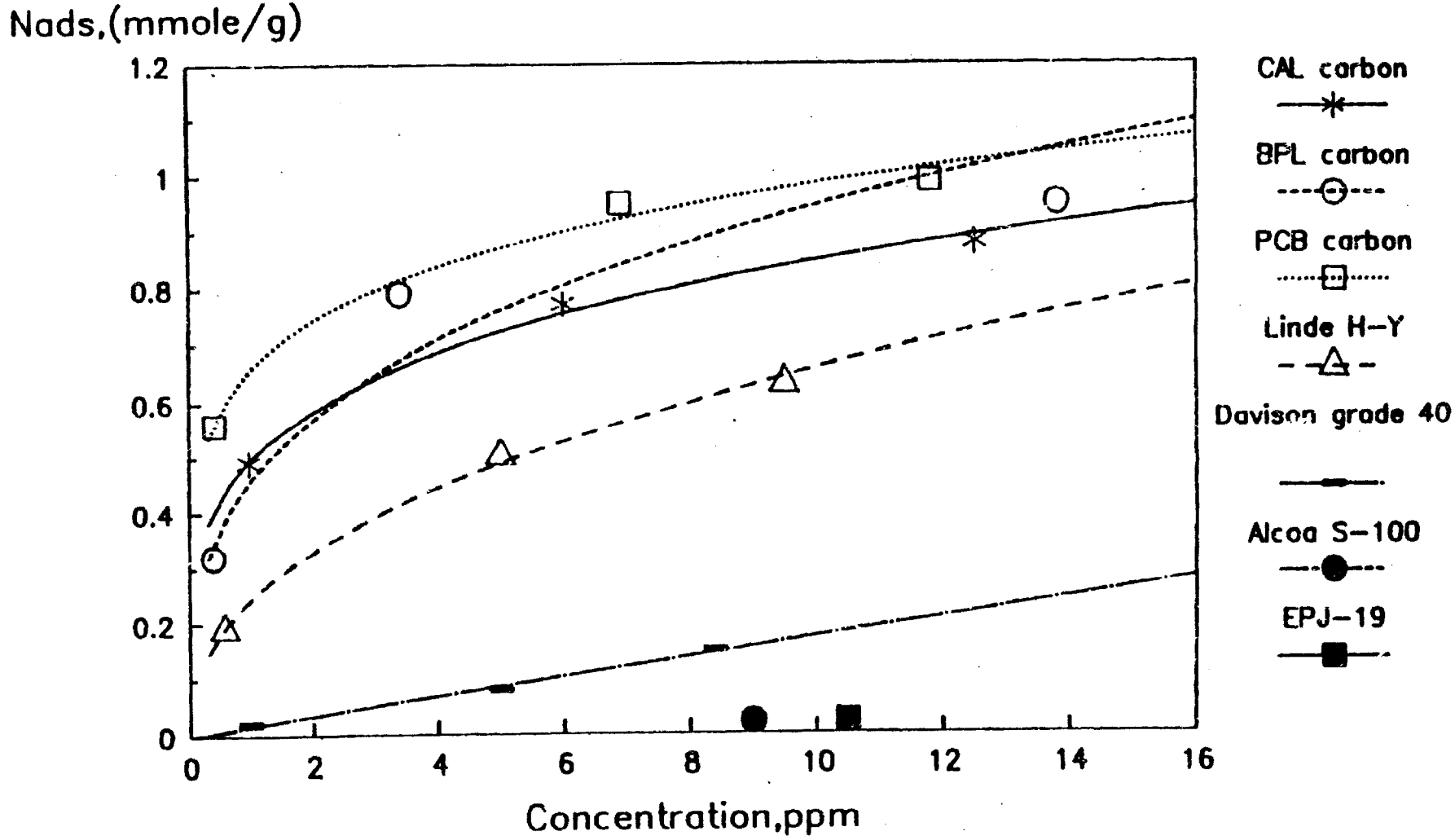

$Fe(CO)_5$ on these adsorbents is dominated by the nature of the pore structure and less effected by the chemical nature of the surface.

Effect of Carrier Gas on $Fe(CO)_5$ Adsorption

The composition of carrier gas has a large effect on the adsorption of trace compounds. As the strength of adsorption between adsorbent and carrier gas increases, the extent of adsorption of the trace impurity decreases. Consequently, the effect of CO_2 carrier gas on the adsorption of $Fe(CO)_5$ on activated carbon and H-Y zeolite was investigated. Of all the compounds present in synthesis gas, CO_2 is most strongly physically adsorbed and therefore its effect was investigated.

Figures 3 and 4 show the effect of CO_2 on the adsorption of $Fe(CO)_5$ on BPL carbon and H-Y zeolite. The reason H-Y zeolite was chosen for this application is that its affinity for CO_2 is much less than that for other zeolites. It is clear from the isotherms that the presence of CO_2 does reduce the $Fe(CO)_5$ capacity of both adsorbents. The capacities of BPL carbon and H-Y zeolite are reduced by about 30% and 50%, respectively, at an equilibrium concentration of 5 ppm $Fe(CO)_5$. The reduction in capacity is greater for the zeolite because CO_2, which is a polar molecule, is adsorbed more strongly on the polar zeolite than the non-polar carbon.

Effect of Temperature on $Fe(CO)_5$ Adsorption at 40 psig

The effect of temperature on $Fe(CO)_5$ adsorption on H-Y zeolite and BPL carbon was investigated. Since adsorption is an exothermic process, the

FIGURE 3

Effect of CO2 on Fe(CO)5 Adsorption on BPL

100 F, 40 psig

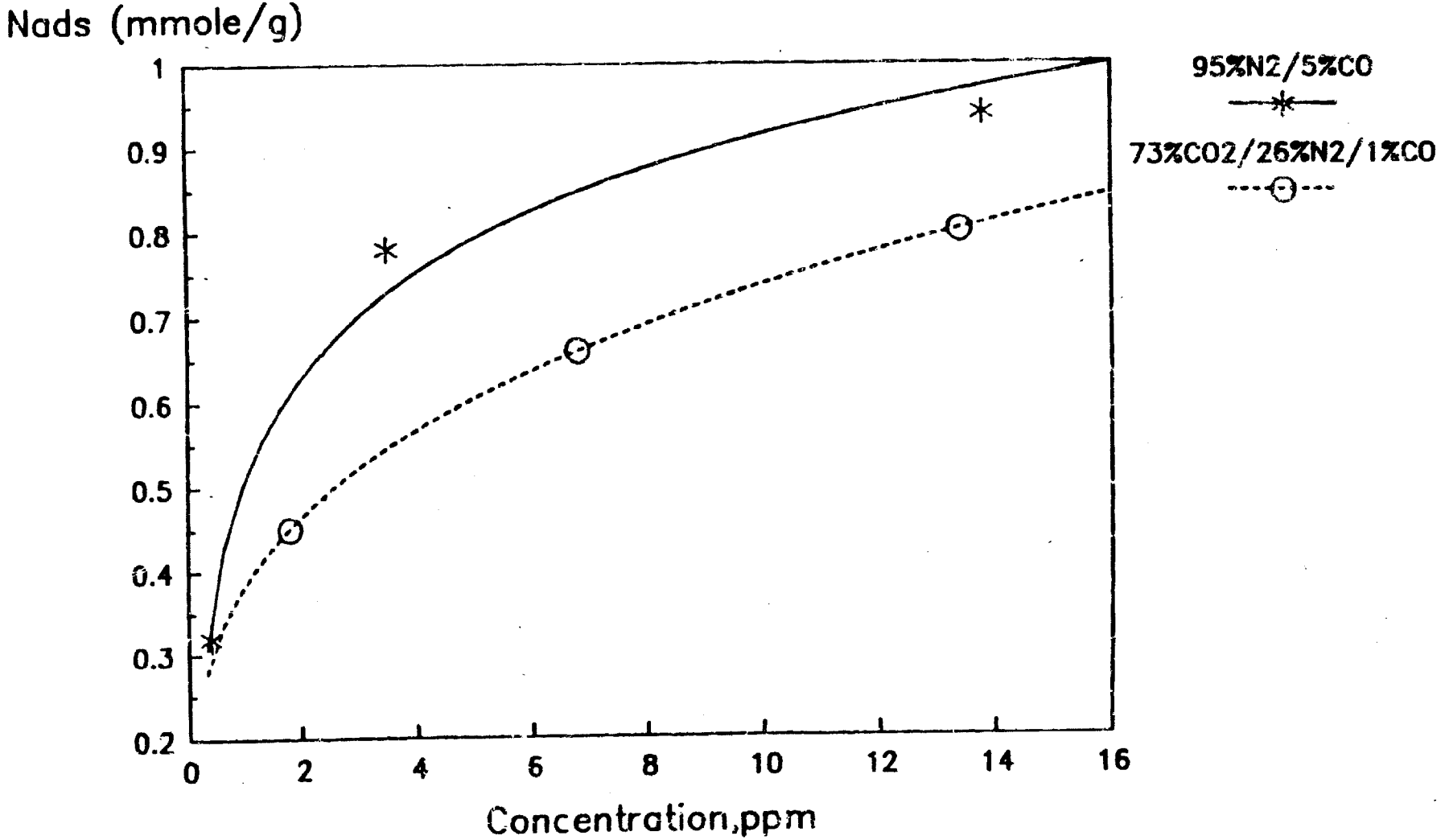

FIGURE 4

Effect of CO2 on Fe(CO)5 Adsorption on H-Y

100 F, 40 psig

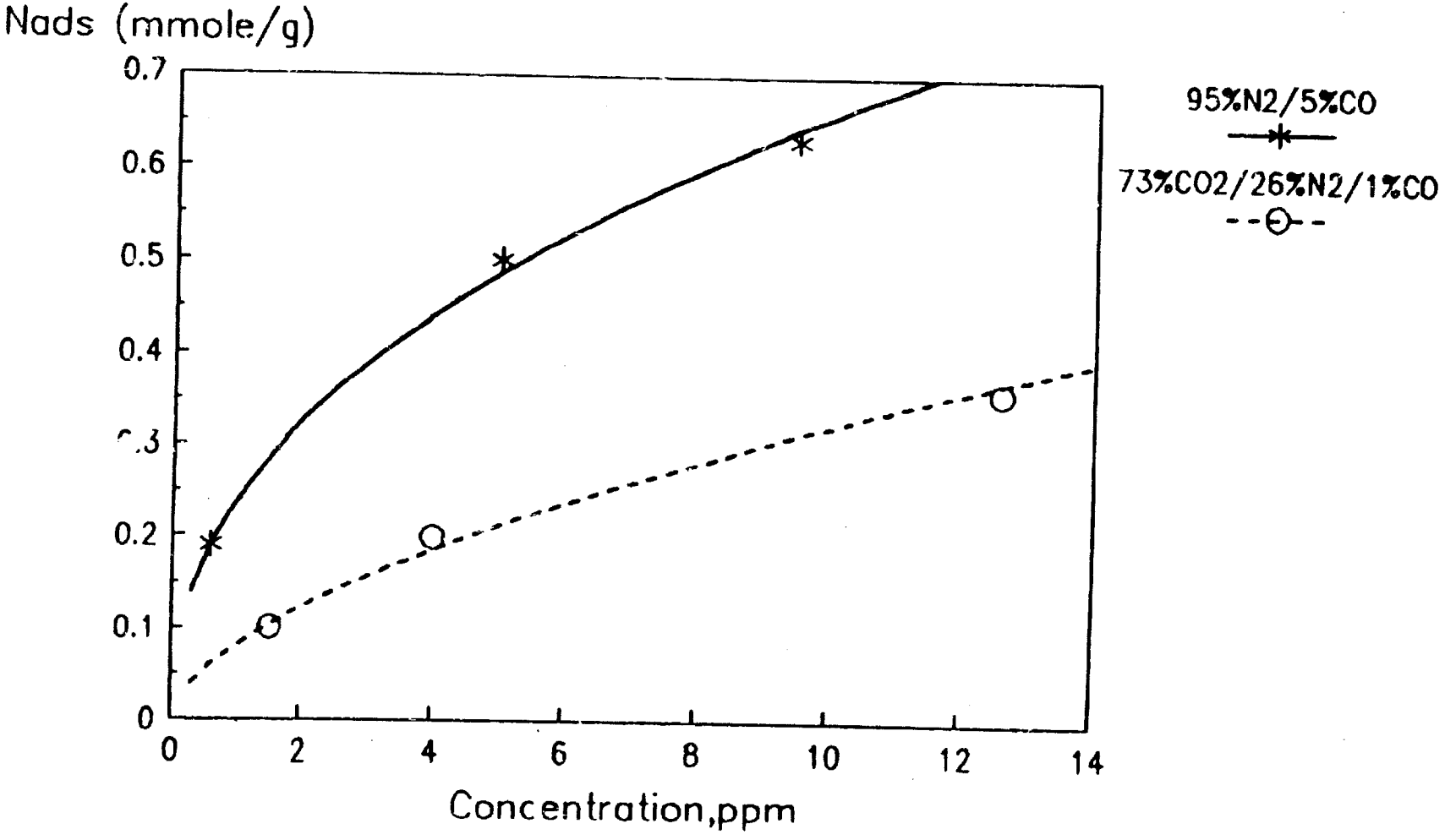

extent of adsorption increases as the temperature decreases. Using the Clausius-Clayperon equation, the isosteric heat of adsorption of a given species can be calculated from isotherms at two different temperatures. The working equation is:

$$\ln(P_1/P_2)_n = qst/R\ (1/T_1 - 1/T_2)$$

where P_1 and P_2 are the partial pressures of the adsorbate at a given amount adsorbed (n) at absolute temperatures T_1 and T_2; qst is the isosteric heat of adsorption and R is the gas constant. In addition, once the heat of adsorption is known as a function of the amount adsorbed, adsorption isotherms at other temperatures can be calculated. It should be emphasized that use of the Clausius-Clayperon equation is strictly thermodynamically correct for pure components only. Hence, the heat of adsorption calculated from mixture data is an "apparent" heat of adsorption. Nonetheless, the technique is useful in estimating the effect of temperature on adsorption.

Figures 5 and 6 show $Fe(CO)_5$ adsorption isotherms at 100 and 75°F from 40 psig (73% CO_2/26% N_2/1% CO) carrier on H-Y and BPL, respectively. In each figure the apparent heat of adsorption as a function of amount adsorbed is given.

Figure 5 shows that the apparent heat of $Fe(CO)_5$ adsorption on Linde H-Y under the given conditions is 12.5 kcal/mole at a surface coverage of 0.10 mmole/g and reduces to 9.6 kcal/mole at 0.30 mmole/g. First, the magnitude of the apparent heat of adsorption is rather large. This indicates that the adsorption of $Fe(CO)_5$ is very sensitive to temperature. For

FIGURE 5

Fe(CO)5 Adsorption at 100 and 75 F on H-Y

40 psig (73%CO2/26%N2/1%CO)

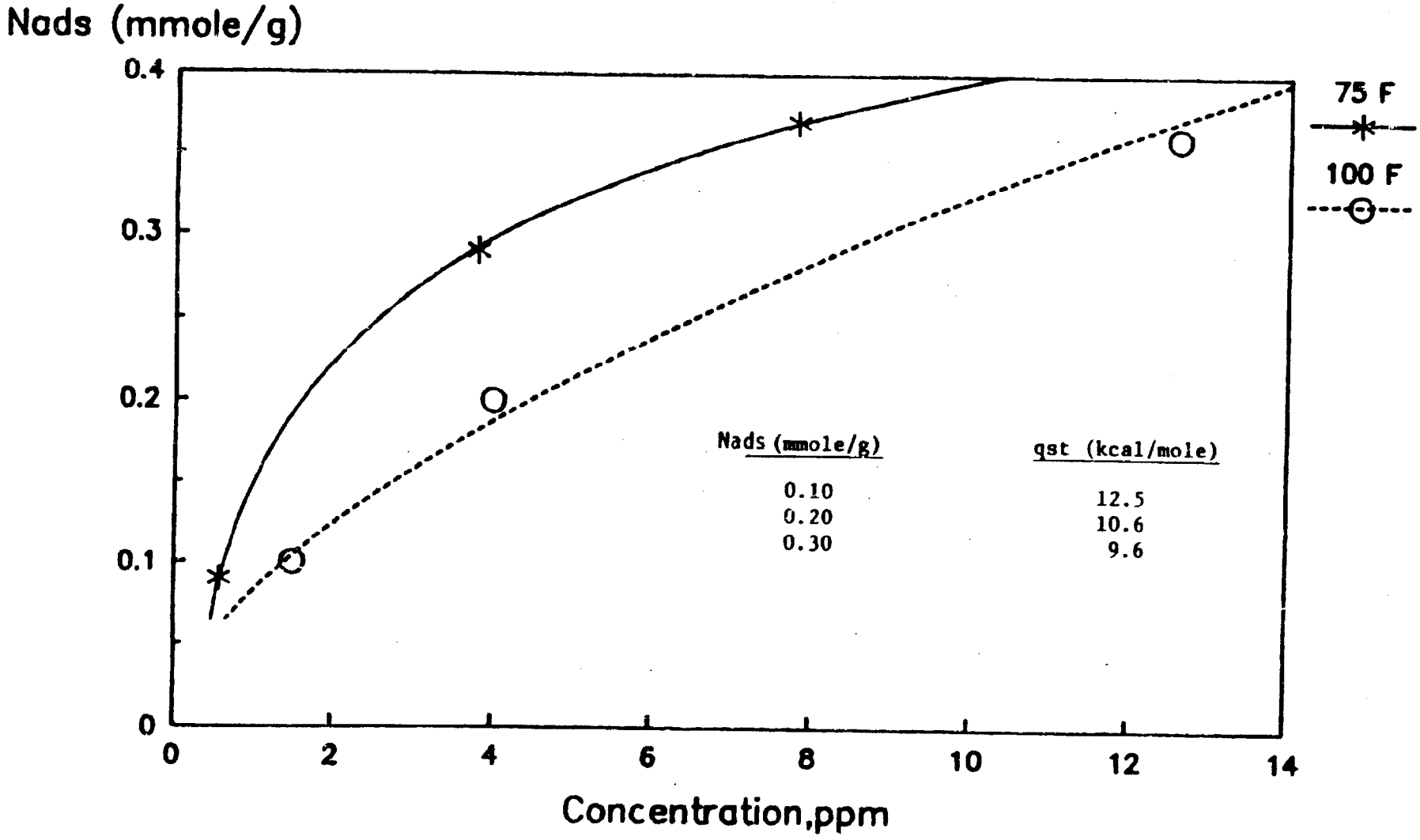

FIGURE 6

Fe(CO)5 Adsorption at 100 and 75 F on BPL

40 psig (73%CO2/26%N2/1%CO)

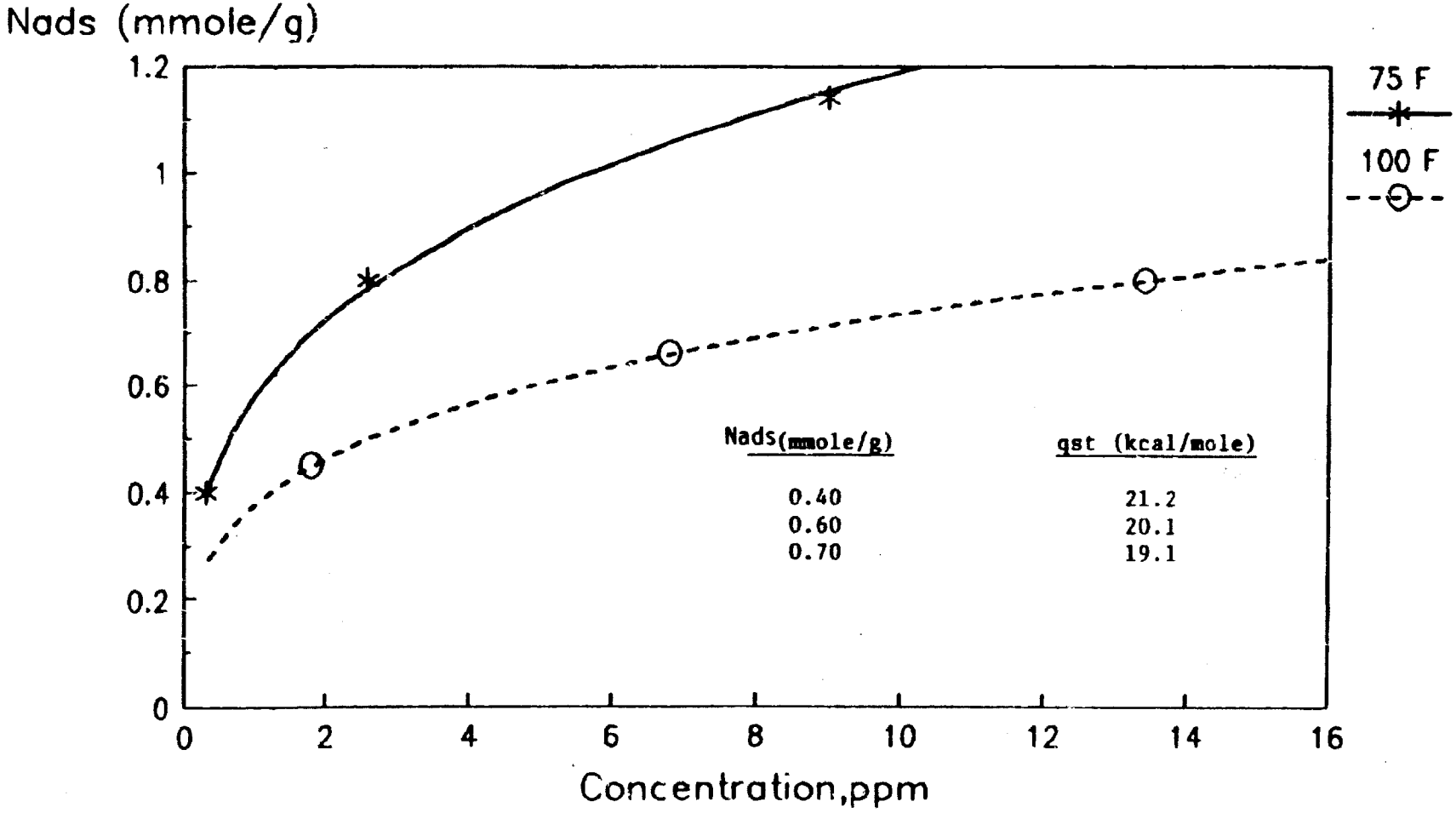

example, at 100°F the adsorption capacity at an equilibrium concentration of 5 ppm is 0.22 mmole/g, while at 75°F that value increases almost 50% to 0.32 mmole/g. Thus, the extent of $Fe(CO)_5$ adsorption can be significantly modified by changing the adsorption temperature. Second, the decrease in apparent heat of adsorption with increasing surface coverage indicates adsorbent heterogenity with respect to $Fe(CO)_5$ adsorption.

Figure 6 shows $Fe(CO)_5$ adsorption isotherms at 100 and 75°F on BPL carbon. Adsorption of $Fe(CO)_5$ on BPL carbon shows greater temperature sensitivity than that on H-Y zeolite as noted by its higher apparent heat of adsorption. The magnitude of the heat of adsorption, ~20 kcal/mole, is very high suggesting that $Fe(CO)_5$ may be chemisorbed on the carbon surface. The heat of adsorption of a compound is an indication of the strength of the adsorption bond. Clearly, $Fe(CO)_5$ is adsorbed more strongly on BPL carbon than H-Y zeolite as evidenced by its adsorption capacity, Henry's law constant and heat of adsorption. The Henry's law constant of an isotherm is proportional to the heat of adsorption. At an equilibrium concentration of 5 ppm, the $Fe(CO)_5$ adsorption capacity at 100°F is 0.62 mmole/g, while at 75°F that value is 0.96 mmole/g. Hence, due to the high heat of adsorption of $Fe(CO)_5$ on both H-Y and BPL, the adsorption capacity can be significantly enhanced by reducing the adsorption temperature.

Thermal Regeneration Studies

The adsorption capacity of BPL carbon at 75°F and 40 psig carrier (73% CO_2/26% N_2/1% CO) is 0.96 mmole/g at an equilibrium concentration of 5 ppm. For a methanol plant with an inlet flow rate of 40 MMSCFD (100 TPD

methanol), the calculated weight of BPL carbon needed to remove 5 ppm $Fe(CO)_5$ based on the above capacity is about 500 lbs of carbon per day. This carbon utilization rate is too expensive for a throw-away adsorbent. Subsequently, regeneration experiments were carried out to determine 1) if the adsorptive capacity of the adsorbents are recovered after thermal regeneration, 2) what temperature is required to regenerate the adsorbent, and 3) if all the carbonyl impurity is desorbed as such or if metal species are deposited on the adsorbent surface.

Figure 7 shows $Fe(CO)_5$ adsorption isotherms on BPL carbon at 75°F from 40 psig carrier (73% CO_2/26% N_2/1% CO) on successive runs following regeneration in N_2 at 250°F. It can be noted that the $Fe(CO)_5$ capacity of BPL is reduced on each successive run following regeneration in N_2 at 250°F. The $Fe(CO)_5$ adsorption capacity at 5 ppm decreases from 0.96 to 0.77 mmole/g following two regeneration cycles.

To help elucidate the cause of this adsorbent deactivation, the gas effluent during regeneration in N_2 was monitored for $Fe(CO)_5$ concentration. By knowing the gas effluent rate and the $Fe(CO)_5$ effluent concentration as a function of time, a desorption curve can be obtained. From this desorption curve, the total quantity of $Fe(CO)_5$ desorbed from the adsorbent can be determined. The $Fe(CO)_5$ desorption curve for BPL carbon is shown in Figure 8. Since the $Fe(CO)_5$ loading of the adsorbent prior to regeneration was known and the total quantity of $Fe(CO)_5$ desorbed can be calculated from the desorption curve, the amount of iron remaining on the carbon surface can be calculated by subtraction.

FIGURE 7

Effect of Regeneration on Fe(CO)5 Capacity

75 F and 40 psig on BPL

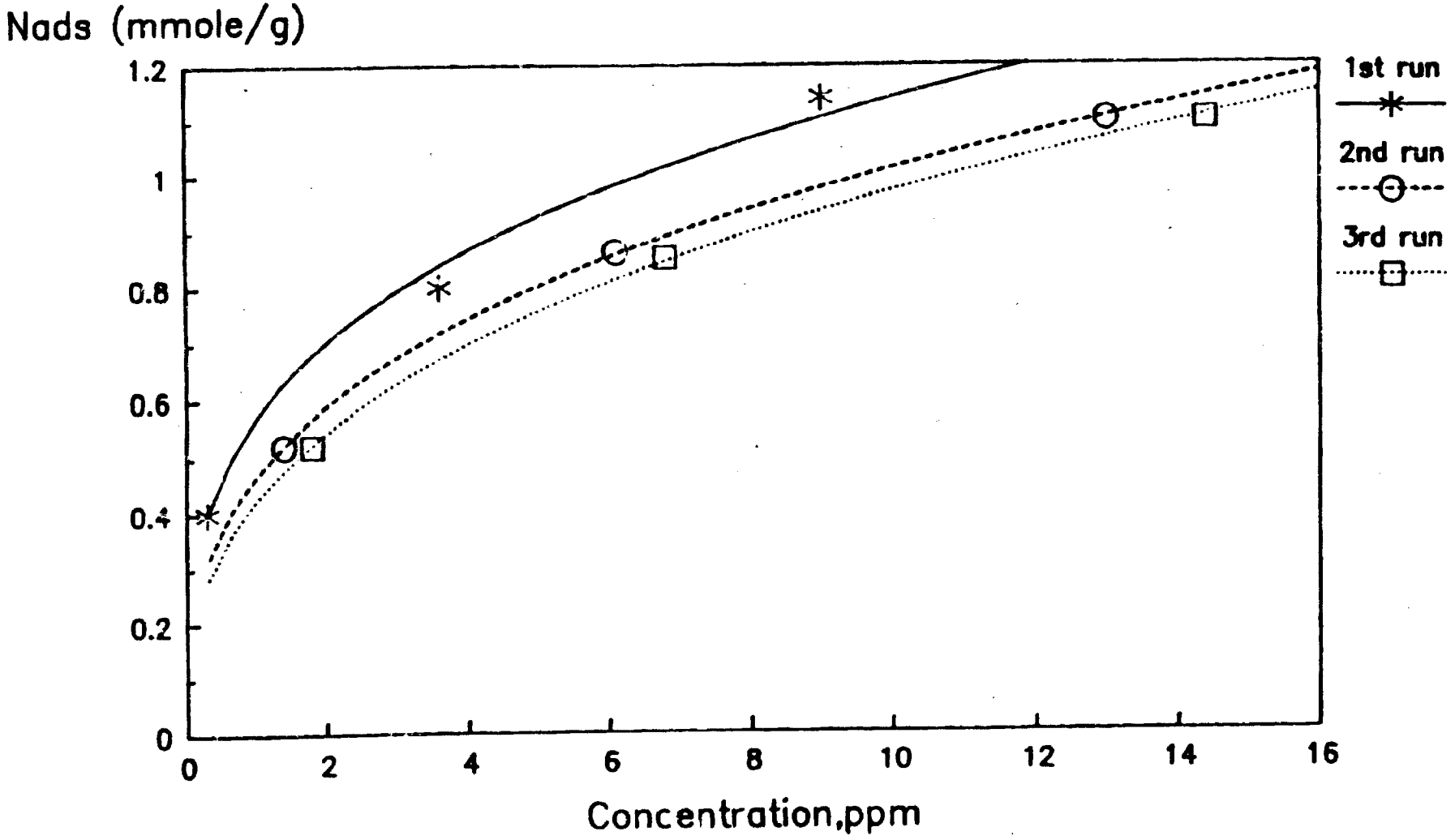

FIGURE 8

Fe(CO)5 Thermal Desorption Curve on BPL

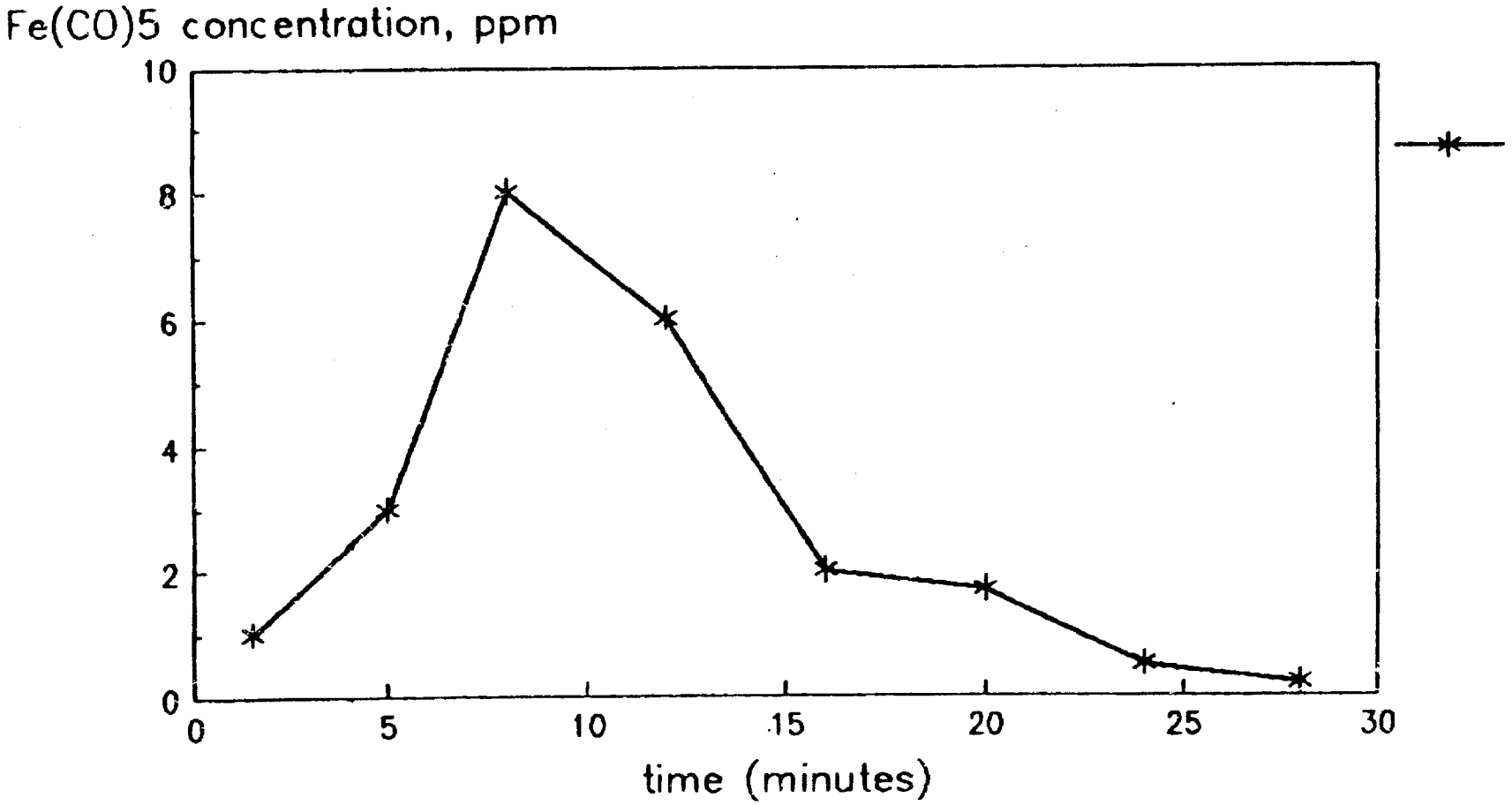

heat rate = 10 F/min
flow rate = 1 liter/min
250 F final temperature

A number of points can be made concerning thermal adsorption of $Fe(CO)_5$ from active carbon. Very little adsorbed $Fe(CO)_5$ is desorbed as $Fe(CO)_5$. The desorption curves indicate that less than 0.1 (wt%) of $Fe(CO)_5$ is desorbed as such. This means a large fraction of some iron species remains on the carbon surface. It is strongly suspected that the iron species is iron metal even though 250°F is below the decomposition temperature (300°F) of $Fe(CO)_5$. Adsorbed $Fe(CO)_5$ can decompose before the decomposition temperature of the pure compound because they are two different thermodynamic species. The "spent" adsorbent is weighed after regeneration and the weight increase is noted. In order to close the mass balance, the weight increase must be done to elemental iron. In addition, other studies on the adsorption of $Fe(CO)_5$ on adsorbents indicate that elemental iron is left on the adsorbent surface following thermal regeneration in this temperature range (3). Other interesting experimental observations which suggest elemental iron is formed in the ferromagnetic nature of the spent adsorbent which is readily attracted to a bar magnet. In addition, both CO and CO_2 are evolved during the thermal decomposition step. It is well known that elemental iron is a catalyst for the Bouduoard reaction at low temperatures (100°C) ($2\ CO \longrightarrow CO_2 + C$)(4). Thus, CO evolved during decomposition of $Fe(CO)_5$ must react in the presence of elemental iron and form CO_2 and deposit carbon. Thus, thermal regeneration studies on active carbon following $Fe(CO)_5$ adsorption demonstrate 1) $Fe(CO)_5$ adsorption capacity is reduced following thermal regeneration, and 2) thermal regeneration leads to deposition of elemental iron on the surface of the carbon which is most likely the reason for the loss of adsorption capacity.

Figure 9 shows $Fe(CO)_5$ adsorption isotherms on Linde H-Y zeolite at 75°F from 90 psig carrier (73% CO_2/26% N_2/1% CO) on successive runs following regeneration in N_2 at 250°F. It is noted that for three successive adsorption/regeneration cycles, the zeolite demonstrates the same adsorptive capacity. A desorption curve similar to that for BPL was measured as shown in Figure 10. It can be noted that significantly more $Fe(CO)_5$ is desorbed from the zeolite than the carbon. However, the total quantity of $Fe(CO)_5$ desorbed is equal to about 30% of that adsorbed. Once again the iron species on the "spent" adsorbent seems to be elemental iron as indicated by mass balance requirements, the ferromagnetic property of the spent adsorbent, and previous investigations of $Fe(CO)_5$ adsorption and decomposition on H-Y zeolite (3).

This raises the question as to why the equilibrium capacity remains the same while iron species are deposited on the zeolite surface? A possible explanation is that the adsorbed $Fe(CO)_5$ in the zeolite pores migrates into the macroporous binder of the zeolite during thermal regeneration. The macropores of the zeolite don't contain significant adsorption capacity. However, diffusion in pelletized zeolites is limited by macropore diffusion. The primary reason for this is the much smaller size of the microporous zeolite crystals (1-10 microns) versus the size of the macroporous binder network (1-2 mm). Hence, if deposition occurs in the macropores, the rate of $Fe(CO)_5$ adsorption should decrease. Figure 11 shows the fractional approach to equilibrium as a function of time on three successive adsorption/regeneration cycles. As depicted in the figure, the approach to equilibrium is slowed with each successive adsorption/regeneration cycle. In addition, previous researchers have shown that the iron crystallites present

FIGURE 9

Effect of Regeneration on Fe(CO)5 Capacity

75 F and 40psig on H-Y

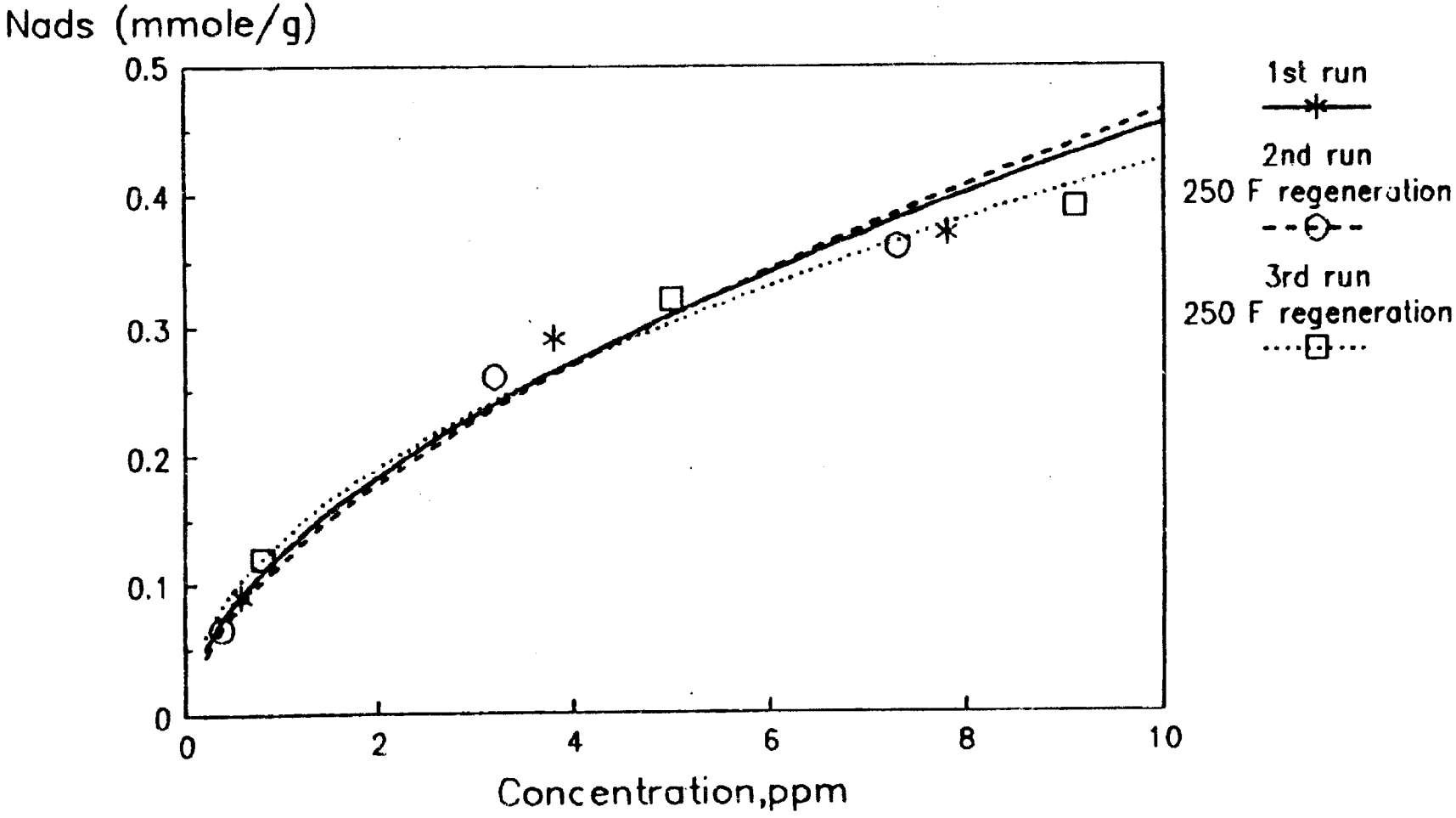

FIGURE 10

Fe(CO)5 Thermal Desorption Curve on H-Y

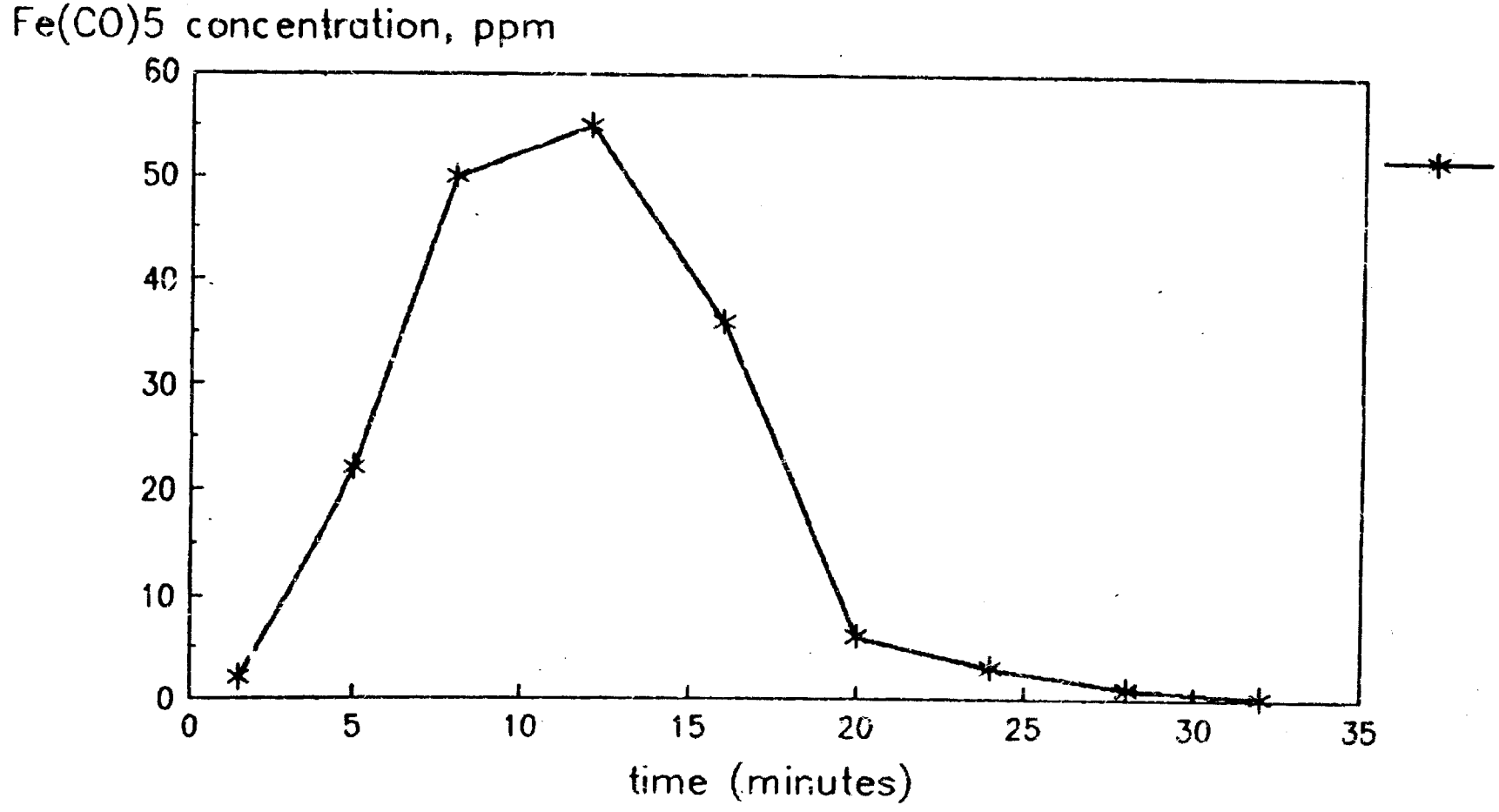

heat rate = 10 F/min
flow rate = 1 liter/min
250 F final temperature